Electron density profiles in the equatorial *E* region ionosphere derived from a bistatic coherent scatter radar experiment in Perú

E. B. Shume and D. L. Hysell

Department of Earth and Atmospheric Sciences, Cornell University, Ithaca, New York, USA

J. L. Chau

Radio Observatorio de Jicamarca, Instituto Geofísico del Perú, Lima, Peru

Received 8 October 2004; revised 26 November 2004; accepted 10 December 2004; published 14 January 2005.

[1] A new bistatic radar system has been developed at the Jicamarca Radio Observatory. The system is a permanent addition to the facility designed to monitor electron density profiles in the equatorial electrojet region using a coherent scatter radar technique that utilizes the Faraday rotation of the scattered signal. A series of radar experiments has been conducted at Jicamarca since March, 2004. In this report, representative *E* region electron density profiles of the equatorial ionosphere are presented. We compare our electron density estimates with: theoretical electron densities derived from the Chapman production function, electron densities measured by rocket experiments, the International Reference Ionosphere (IRI-2001) model, and peak electron density estimates from the Jicamarca Digisonde. Overall, the radar measured density profiles have magnitudes and shapes comparable to the electron density estimators mentioned above. However, the measured and IRI-2001 model density profiles disagree significantly below the *E* region peak. **Citation:** Shume, E. B., D. L. Hysell, and J. L. Chau (2005), Electron density profiles in the equatorial *E* region ionosphere derived from a bistatic coherent scatter radar experiment in Perú, *Geophys. Res. Lett.*, *32*, L01107, doi:10.1029/2004GL021715.

1. Introduction

[2] The intense Hall current flowing at the magnetic equator causes the *E* region equatorial ionosphere to be unstable, producing a broadband spectrum of field-aligned plasma waves [*Farley*, 1985]. The fact that the electrojet medium is governed by nonthermal physics makes the application of incoherent scatter radar techniques for extracting ionospheric plasma parameters impossible. However, the common presence of nonthermal fluctuations, triggered by gradient-drift and Farley-Buneman instabilities, furnishes a medium for coherent scatter radar diagnostics. *Hysell and Chau* [2001] designed a bistatic coherent scatter radar system that exploits the strong echoes from electrojet irregularities to infer *E* region electron density profiles from the Faraday rotation of the scattered signal.

[3] The bistatic radar geometry has two simultaneous merits: (i) the Bragg scattering vector is normal to the geomagnetic field such that coherent echoes from field aligned electrojet irregularities can be detected, and (ii) the wave undergoes a considerable amount of Faraday rotation while traversing the *E* region ionosphere [*Hysell and Chau*, 2001]. Unlike monostatic radar experiments, however, in a bistatic radar geometry, Bragg's condition for constructive interference permits more than one spatial (Fourier) scattering component; the magnitude of the scattering vector depends on the scatterer altitude. In other words, the spatial length of the scatterer is unique to each radar range gate.

[4] The quasi-longitudinal theory of electromagnetic wave propagation in a cold magnetoplasma is the foundation for estimating electron density in the bistatic radar experiment. The theory relates the Faraday angle to the electron density of the medium quantitatively. The validity of the theory applied to the equatorial electrojet region was tested in a trial experiment conducted in September of 2000 at the Jicamarca Radio Observatory (JRO) near Lima, Peru [*Hysell and Chau*, 2001].

[5] Since March of 2004, a series of bistatic radar experiments has been conducted between JRO and Paracas, Peru, utilizing the newly installed radar system. In this manuscript, we report on daytime *E* region electron density measurements in the equatorial ionosphere inferred from the data of March 23, 2004. We show altitudinal and temporal variations of the *E* region electron density near the magnetic equator. Electron density estimates from the radar experiment are compared and contrasted with electron density profiles calculated from the Chapman production function, electron density profiles derived from rocket experiments carried out in Thumba, India, the International Reference Ionosphere (IRI-2001) model, and *E* region peak density estimates from the Jicamarca Digisonde. Overall, *E* region electron densities inferred from the bistatic data agree satisfactorily with the theoretical and experimental electron density estimates mentioned above. It is noteworthy, however, that below the altitude of the *E* region peak, the measured density profiles diverge significantly from the IRI-2001 profiles.

2. Bistatic Radar Observations

[6] The transmitter for the bistatic radar system is located at Jicamarca, and the receiver is located about 2° south in Paracas, Peru. The transmitter and receiver coordinates and a summary of the radar operating parameters for both the new and original radar systems are shown in Table 1. In order to enhance the sensitivity of the system, (i) the transmitter and receiver of the original bistatic system were swapped in order to be able to utilize two 30 kW trans-

0094-8276/05/2004GL021715$05.00

Table 1. The Current and Original Bistatic Radar Operating Modes

Parameters	Current Experiments	2000 Experiments
Frequency, MHz	49.92	49.92
Peak power, kW	60	20
IPP,[a] μs	2500	250
Coherent integrations	16	8
Pulse width, μs	4 × 13 BC[b]	3
Range resolution, m	600	450
Altitude resolution, m	840–900	630–680
Range gates	92	40
HPFBW[c]	4°	6°
Transmitter coordinates	11°57′S 76°52.6′W	13°51′S 76°14.96′W
Receiver coordinates	13°51′S 76°14.96′W	11°57′S 76°52.6′W
Antenna	Sixteen five element Yagis 0.7λ spacing	Four five element Yagis 1.5λ spacing

[a]Inter Pulse Period.
[b]Barker Code.
[c]Half Power Full Beam Width.

mitters available at Jicamarca, thus increasing the peak power by a factor of 3, (ii) the transmitting and receiving antenna arrays were enlarged in order to suppress grating sidelobes and, at the same time, enhance the signal strength at the receiver, and (iii) Barker coded pulses were introduced. The system upgrades provide close to 20 dB improvement in sensitivity.

[7] Figure 1a shows electron density measurements (circles) with errors bars derived from the radar experiment. The coherent scatter radar experiment has enabled us to measure electron density profiles spanning about 14 km altitude in the electrojet region. With the exception of the extreme top and bottom altitudes, the densities were measured with a high degree of accuracy; relative uncertainties were only 0.7% on average.

[8] Figure 1a shows that the plasma density scale height has distinct values below and above the peak, having a relatively small magnitude below the peak compared to above the peak (and leading to the valley region). This feature is shared by *E* region density profiles in the midlatitude [*Trost*, 1979] and high latitude [*Brekke and Hall*, 1988] ionospheres.

[9] The waterfall plot in Figure 2 shows the altitudinal variation of the measured electron density in the equatorial electrojet region as well as its temporal variation from 9:00 to 16:00 local time. Both the bottomside and topside coherent radar returns underlying the density profiles are due to short wavelength irregularities in the electrojet. *Kudeki et al.* [1987] have suggested that pure two-stream processes provide the mechanism for the topside coherent scatter. The bottomside irregularities are explained by a gradient drift wave driven mode coupling mechanism [*Sudan and Keskinen*, 1979]. Around noon local time (two hours before and after noon) where the solar zenith angle is minimum, strongly driven pure two-stream waves are present, making topside density measurement possible. The positive density gradient in the bottomside allows gradient-drift wave processes, permitting coherent scatter radar density measurements in the bottomside. However, before 9:45 and after 14:00 local times when the topside echoes subside and bottomside echoes get weaker, the density profiles contract in altitude.

3. Measured Density Profiles Compared With Other Electron Density Estimates

[10] Here, we compare the radar derived equatorial *E* region electron densities with four electron density estimates: theoretical (electron density function derived from the α Chapman production function), experimental (rocket) electron density measurements, International Reference Ionosphere (IRI-2001) model *E* region electron density predictions (the comparisons are shown in Figures 1b–1d,

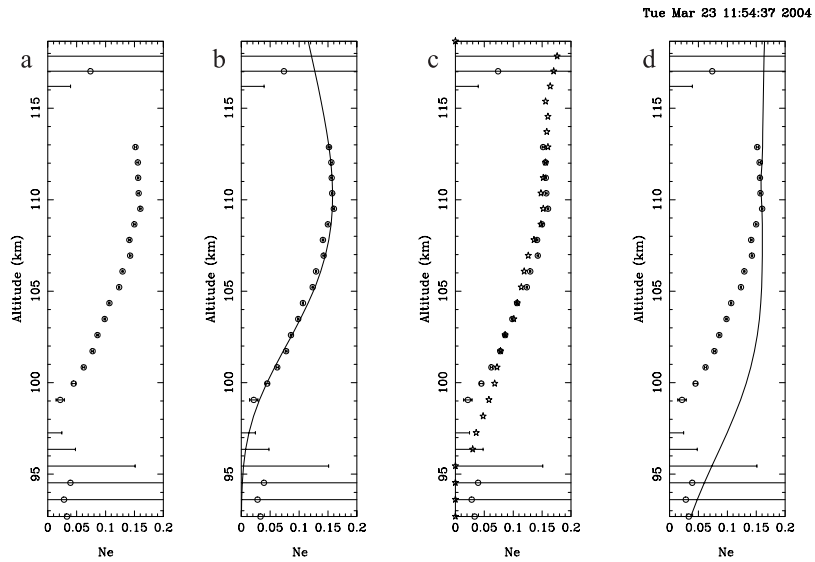

Figure 1. (a) Measured electron density profile with error bars; (b) measured density (circles) superimposed on a Chapman electron density function (solid line); (c) measured density (circles) along with electron density from rocket experiments (stars); (d) measured density (circles) superimposed on IRI-2001 (solid line); All times are local time; Ne (Electron density) in units of $10^6 cm^{-3}$.

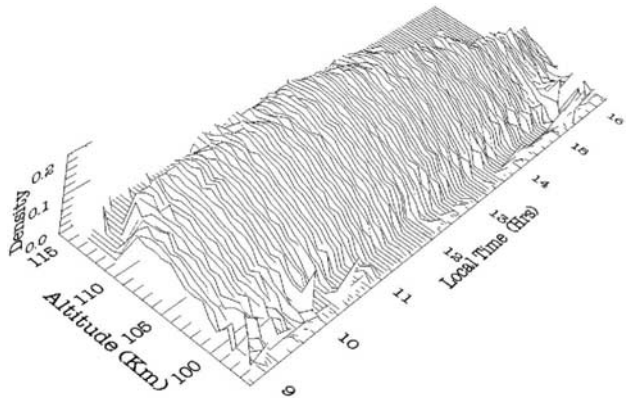

Figure 2. The waterfall plot depicts altitudinal and temporal variations of equatorial *E* region electron density (in units of $10^6 cm^{-3}$) derived from short wavelength coherent scattering in the bistatic radar experiment between Jicamarca and Paracas, Peru on March 23, 2004.

respectively), and peak densities from the Jicamarca Digisonde Portable Sounder (DPS-4) (shown in Figure 3).

3.1. Electron Density Profile From the α Chapman Function

[11] The altitude variation of *E* region electron density can be represented by a simplified electron density function ($N(z)$, z for altitude) derived from the Chapman production function,

$$\frac{N(z)}{N_mE} = \exp\left(\frac{1}{2}(1 - \zeta - \sec(\chi)\exp(-\zeta))\right) \quad (1)$$

where N_mE is peak *E* region electron density, $\zeta = \frac{z - h_mE}{H}$, h_mE is the peak altitude, H is the atmospheric scale height, and χ is the solar zenith angle. The α Chapman function is employed in this case since the loss of ionization content is assumed to behave quadratically in the *E* region ionosphere. Figure 1b shows a superposition of a Chapman electron density function $N(z)$ (solid line) and the measured densities (circles). To calculate $N(z)$, we used $N_mE = 0.161 \times 10^6$ cm^{-3}, $h_mE = 110.0$ km, and $\chi = 14.3°$ at noon local time for March 23, 2004 as obtained from IRI-2001 specifications [*National Space Science Data Center*, 2001], and a constant atmospheric scale height $H = 6.2$ km as derived from the MSIS-E-90 Atmosphere Model [*National Space Science Data Center*, 1990]. Appreciable congruence is found between bistatic data and the theoretical density, $N(z)$.

3.2. Electron Density From Rocket Measurements

[12] A full solar cycle of equatorial daytime *E* region electron density data from Langmuir probes onboard rocket flight experiments in Thumba (India) is represented in Figure 7 of *Chandra et al.* [2000]. Here in Figure 1c, we have reproduced an electron density profile (stars) from a rocket flight experiment conducted in the spring of 1975 representing solar minimum conditions. The shape and magnitude of our measured density profile (circles) are comparable to the rocket probe data except around the very lowest altitudes where the radar measurement has significant uncertainty.

3.3. Electron Density From IRI-2001 Ionospheric Parameter Specifications

[13] We have also made a comparison of the IRI-2001 *E* region electron density predictions [*Bilitza*, 2001] with the radar derived densities. IRI-2001 results (solid line) superimposed on the density measurements (circles) for March 23, 2004 at noon are shown in Figure 1d.

3.3.1. At and Above the Peak

[14] Figure 1d clearly demonstrates that at and above the peak, the IRI-2001 and measured densities are coincident. The IRI peak density model is constructed utilizing a worldwide network of ionosonde f_oE (*E* region critical plasma frequency) measurements [*Bilitza et al.*, 1993; *Bilitza*, 2001], hence the reason for the good agreement between the IRI and measured peak values. In addition, in both the IRI and measured density profiles, the peak density occurred at 110.0 km. In general, the radar measured density peak altitude varies between 108.0 km and 111.0 km (not shown here), the typical peak altitude being 110.0 km.

3.3.2. Below the Peak

[15] However, the two electron density estimates depart drastically below the peak. The IRI bottomside *E* region density profile is represented by an arbitrary exponential function that connects the *D* region to the *E* region peak density [*Bilitza*, 1990]. Mathematically, there might be multiple ways of smoothly joining the *D* region and *E* region peaks. The discrepancy mentioned above can be attributed to the fact that IRI bottomside *E* region profile is an arbitrary mathematical function which does not have an observational basis. Evidently, the IRI model overestimates *E* region bottomside electron densities as shown in Figure 1d.

3.4. Peak Density Comparison

[16] The Jicamarca Digisonde Portable Sounder (DPS-4) records f_oE at 15 minute intervals. At noon on March 23, 2004, $f_oE = 3.62$ MHz, and the corresponding peak *E* region electron density was $N_mE = 0.162 \times 10^6$ cm^{-3}. The peak IRI electron density was (0.161×10^6 cm^{-3}). On the same day at local noon, the measured peak density was (0.162 ± 0.001) $\times 10^6$ cm^{-3}. Therefore, the peak electron density estimates are in fairly good agreement, their difference falling within the range of experimental uncertainty.

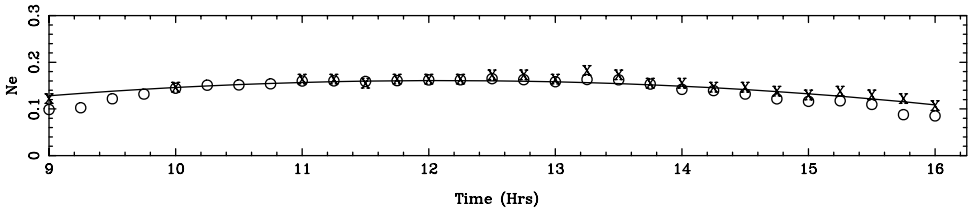

Figure 3. Temporal variation of peak density, radar (circles), the Jicamarca Digisonde (X), and IRI-2001 (solid line) on March 23, 2004; All times are local time; Ne (Electron density) in units of $10^6 cm^{-3}$.

[17] A time series comparing the peak densities is shown in Figure 3. Figure 3 shows how the measured peak density (circles) compares with the Jicamarca Digisonde (X) and IRI-2001 (solid line) peak density estimates. The measured peak is consistent with the Digisonde and IRI peak values from about 10:00 to 14:30 local time. However, about two hours before and after local noon, two stream processes terminate in the electrojet, and because gradient drift processes are stable near and above the *E* region peak by definition, echoes from near and above the peak vanish. The density profiles are accurate but incomplete and are therefore unsuitable for tracking the altitude or density of the peak throughout the day.

4. Conclusion

[18] We have reported equatorial *E* region electron density profiles measured with a new bistatic radar system at Jicamarca and Paracas, Peru. The radar measurements agree well with other electron density estimates. Data are available only at altitudes and local times when strong plasma irregularities are present, limiting their usefulness in certain kinds of statistical studies and making then unsuitable, for instance, for tracking the *E* region peak altitude over time. The bistatic system is now permanently installed at Jicamarca and Paracas for continuously monitoring electron density profiles in the equatorial electrojet region. The *E* region electron densities will be deposited in the CEDAR database for use by the space physics community.

[19] **Acknowledgments.** The authors would like to thank Professor H.S.S.Sinha of the Physical Research Laboratory, Ahmedabad (India) for his help in providing the rocket experiment electron density data. This work was supported by the National Science Foundation through cooperative agreement ATM-9911209 to Cornell University and by NSF grant ATM-0226235 to Cornell University. The Jicamarca Radio Observatory is operated by the Instituto Geofísico del Perú, Ministry of Education, with support from the NSF cooperative agreements just mentioned. The help of the staff was much appreciated.

References

Bilitza, D. (1990), International reference ionosphere 1990, *NSSDC 90-22*, Natl. Space Sci. Data Cent., Greenbelt, Md.

Bilitza, D. (2001), International reference ionosphere 2000, *Radio Sci.*, *36*(2), 261.

Bilitza, D., K. Rawer, L. Bossy, and T. Gulyaeva (1993), International reference ionosphere: Past, present, future: I. Electron density, *Adv. Space Res.*, *13*(3), 3.

Brekke, A., and C. Hall (1988), Auroral ionospheric quiet summer time conductance, *Ann. Geophys.*, *6*(4), 361.

Chandra, H., H. S. S. Sinha, and R. G. Rastogi (2000), Equatorial electrojet studies from rocket and ground measurements, *Earth Planets Space*, *52*, 111.

Farley, D. T. (1985), Theory of equatorial electrojet plasma waves: New developments and current status, *J. Atmos. Terr. Phys.*, *42*, 729.

Hysell, D. L., and J. L. Chau (2001), Inferring *E* region electron density profiles at Jicamarca from Faraday rotation of coherent scatter, *J. Geophys. Res.*, *106*, 30,371.

Kudeki, E., B. G. Fejer, D. T. Farley, and C. Hanuise (1987), The Condor equatorial electrojet campaign: Radar results, *J. Geophys. Res.*, *92*, 13,561.

National Space Science Data Center (1990), MSIS-E-90 atmosphere model, http://nssdc.gsfc.nasa.gov/space/model/models/msis.html, Greenbelt, Md.

National Space Science Data Center (2001), International reference ionosphere: IRI-2001, http://nssdc.gsfc.nasa.gov/space/model/models/iri.html, Greenbelt, Md.

Sudan, R. N., and M. J. Keskinen (1979), Theory of strongly turbulent two-dimensional convection of low-pressure plasma, *Phys. Fluids*, *22*, 2305.

Trost, T. F. (1979), Electron concentrations in the *E* and upper *D* region at Arecibo, *J. Geophys. Res.*, *94*, 6.

J. L. Chau, Radio Observatorio de Jicamarca, Instituto Geofísico del Perú, Apartado 13-0207, Lima 13, Perú. (jchau@jro.igp.gob.pe)

D. L. Hysell, Department of Earth and Atmospheric Sciences, Cornell University, 2108 Snee Hall, Ithaca, NY 14853, USA. (dlh37@cornell.edu)

E. B. Shume, Department of Earth and Atmospheric Sciences, Cornell University, 2159 Snee Hall, Ithaca, NY 14853, USA. (ebs27@cornell.edu)